A robust optimal control framework for controlling aberrant RTK signaling pathways in esophageal cancer

Souvik Roy *†¶ Zui Pan ‡¶ Naif Abu Qarnayn†¶ Mesfer Alajmi †¶ Ali Alatwi †¶ Asma Alghamdi †¶ Ibrahem Alshaoosh †¶ Zahra Asiri †¶ Berlinda Batista †¶ Shreshtha Chaturvedi †¶ Olusola Dehinsilu †¶ Hussein Edduweh †¶ Rodina El-Adawy †¶ Emran Hossen †¶ Bardia Mojra §¶ Jashmon Rana †¶

Abstract

This study presents a new framework for obtaining personalized optimal treatment strategies targeting aberrant signaling pathways in esophageal cancer, such as the epidermal growth factor (EGF) and vascular endothelial growth factor (VEGF) signaling pathways. A new pharmacokinetic model is developed taking into account specific heterogeneities of these signaling mechanisms. The optimal therapies are designed to be obtained using a three step process. First, a finite-dimensional constrained optimization problem is solved to obtain the parameters of the pharmacokinetic model, using discrete patient data measurements. Next, a sensitivity analysis is carried out to determine which of the parameters are sensitive to the evolution of the variants of EGF receptors and VEGF receptors. Finally, a second optimal control problem is solved based on the sensitivity analysis results, using a modified pharmacokinetic model that incorporates two representative drugs Trastuzumab and Bevacizumab, targeting EGF and VEGF, respectively. Numerical results with the combination of the two drugs demonstrate the efficiency of the proposed framework.

Keywords: optimization, non-linear conjugate gradient, Weibull distribution, monoclonal antibodies, HER2 blockers.

MSC: 34H05, 49J20, 49K20, 62D99, 65L08, 93C10

^{*(}Corresponding Author) souvik.roy@uta.edu

[†]Department of Mathematics, The University of Texas at Arlington, Arlington, TX 76019-0407, USA

[‡]College of Nursing and Health Innovation, The University of Texas at Arlington, Arlington, TX 76019-0407, USA

Department of Computer Science, The University of Texas at Arlington, Arlington, TX 76019-0407, USA

[¶]All authors contributed equally

1 Introduction

Esophageal cancer (EC) is the sixth leading cause of cancer deaths worldwide [19]. It presents no significant symptoms at an early stage and, thus, tends to be diagnosed very late [34]. This leads to very few available treatments for cure or control of EC, leading to a high mortality rate [8]. Thus, the need for development of accurate and timely treatments for EC is crucial. Accumulating evidence has shown abnormal activities in various signaling pathways in a broad range of cancers, which can be targeted as therapy [9, 18, 27, 37, 38, 40]. It is worthwhile to note that all these studies are experimental in nature and are based on data from a limited number of patients. In particular, it has been observed that in EC, several receptor tyrosine kinases (RTKs), such as epidermal growth factor (EGF) receptor, HER2, and vascular endothelial growth factor (VEGF) receptor, present significant increased expression in EC tumor compared to normal tissues [36]. They often presents high copy numbers, which has been found to correlate with poor prognosis and aggressive malignancy. Thus, it is of paramount importance to understand the dynamics of RTK signaling pathways and to develop strategies targeting them in order to combat EC. Many small molecule compounds and monoclonal antibodies targeting RTKs have been developed and some have been approved by FDA for cancer treatment. For example, Trastuzumab and Bevacizumab are two drugs targeting HER2 and VEGF receptors, respectively [11, 22, 23, 24].

To understand the dynamics of RTK signaling pathways, mathematical frameworks are very natural and rich, and can provide a speedy assessment without the need for a large number of clinical trials. One class of mathematical frameworks is the pharmacokinetic models that use differential equations to describe the anatomical, physiological, physical, and chemical processes involved due to the effects of cancer inside a body [4, 41]. These models take into account the molecular characteristics of an individual patient, thus, able to accurately model and predict the cancer progress. Numerous deterministic pharmacokinetic models have been used in past to model the dynamics of RTK signaling pathways for different cancer types. In [3], the authors use a ODE-based model to explore the relationship between EGFR and IGF1R protein expressions in non-small cell lung cancer. A mathematical model for crosstalk between estrogen receptor and EGFR was presented in [5]. In [6, 7], the authors develop ordinary differential equations (ODE)based models for studying the effects of HER2 overexpression on cell proliferation in breast cancer. The authors in [14] present a mathematical model based on ODE to understand the dimerization process for Gefitinib resistance in lung cancer. A computational model was used to simulate the main biochemical and metabolic interactions in the PI3K/AKT and MAPK pathways in melanoma cancer [28]. The authors in [30] study the therapy resistance in RTK signaling pathways through the AKT pathways in colon cancer. To the best of our knowledge, no such model is available for RTK signaling pathways in EC.

Comparing with other solid tumor malignancies, EC patients present much more heterogeneity and diverse cancerogenous origins [39]. There are two primary types of heterogeneities in pathways related to EC: extrinsic and intrinsic [16]. Extrinsic heterogeneities arise due to the fact that the development of EC involves various perturbation events like gene copy number amplification and are also induced by different environmental signals, like metabolic stress, inflammatory microenvironments, immune responses [2]. Intrinsic heterogeneities are a result of intracellular dynamics,

not necessarily related to EC [35]. These heterogeneities have been found to be a major factor in drug resistance in EC. Thus, it is important to develop a pharmacokinetic model that can incorporate heterogeneities in EC. As a simplistic answer to this question, in this paper, we present a new pharmacokinetic model for RTK signaling pathways in EC by modeling interactions between two biological entities using a combination of Michaelis-Menten and Mass action laws. The rationale behind such a modeling is to incorporate a specific kind of extrinsic heterogeneitic behavior, where copies of the same biological entity can behave differently.

Pharmacokinetic models contain a set of parameters that represent important physiological and mechanistic characteristics in a body, like cell counts, absorption rates, diffusion rates, and so on. Accurate estimation of these parameters and determining the most sensitive ones with respect to the EGFR receptors are very crucial in order to devise an appropriate treatment method for the patient. Existing methods of parameter estimation rely on the availability of huge datasets for an accurate estimation. But such large datasets are in scarcity [17]. In this paper, we present a data-driven optimal control framework for devising personalized treatment targeting aberrant pathways using a 3-step process: we first estimate the parameters of our pharmacokinetic model through a finite dimensional optimization framework that yields accurate, robust, and stable estimates of the parameters. Next, we determine which of the parameters are sensitive with respect to EGFRs-dependent tumor growth. We finally, solve an optimal control problem that incorporates combination drugs, based on the sensitivity analysis results, and provides the optimal dosages.

The main content of this paper is divided into six sections. Following the Introduction, Section 2 describes the new pharmacokinetic ODE model for the evolution of the pathways, and present the optimization problems used for obtaining the optimal therapies. Section 3 contains theoretical results related to the pharmacokinetic model and the corresponding optimization problems. Section 4 presents a NSFD numerical scheme for solving the forward and the adjoint ODE systems, and the projected non-linear conjugate gradient (PNCG) method for solving the optimality system. We also present the method for carrying out the sensitivity analysis of the optimal parameter set. Section 5 presents the results of our proposed optimal control framework followed by Section 6: Conclusions and Acknowledgements.

2 A controlled quantitative systems pharmacology model for pathways

We aim at developing a quantitative systems pharmacology (QSP) model for pathway dynamics in a single cancer cell. In the cell, a monovalent EGF ligand (L), binds reversibly to monovalent cell surface EGF receptor (R) to form a receptor-ligand EGFR-EGF complex (C), and this reaction is reversible. The occupied receptor then hetero-dimerizes with the cell surface HER2 receptor to form a dimer or ternary complex EGFR-EGF-HER2 (T), which is also a reversible reaction. Below is the schematic of the reactions:

$$EGFR(R) + EGF(L) \rightleftharpoons EGF : EGFR(C)$$

$$EGF : EGFR(C) + HER2(H) \rightleftharpoons EGF : EGFR : HER2(T)$$

We assume there is no cell proliferation, so that the total number of bound and unbound EGF receptors (R) and HER2 receptors (H) at any given time is conserved. The aforementioned process can be represented through the evolution of the following variables:

- 1. $H(\tau)$ the density of HER2 receptors (#/volume)
- 2. $T(\tau)$ the density of EGF:EGFR:HER2 complex (#/volume)
- 3. $R(\tau)$ the density of EGFR receptors (#/volume)
- 4. $C(\tau)$ the density of EGF:EGFR complex (#/volume)
- 5. $L(\tau)$ the concentration of EGF (μM)

where $\tau(hours)$ is the time variable. The dynamics is given through the governing system of ODEs

$$\frac{d\bar{H}}{d\tau} = -\bar{a}_{1} \frac{\bar{C}\bar{H}}{\bar{K}_{H} + \bar{H}} - \bar{a}_{2}\bar{C}\bar{H} + \bar{a}_{3}\bar{T},
\frac{d\bar{T}}{d\tau} = \bar{a}_{1} \frac{\bar{C}\bar{H}}{\bar{K}_{H} + \bar{H}} + \bar{a}_{2}\bar{C}\bar{H} - \bar{a}_{3}\bar{T} - \bar{\beta}_{1}\bar{u}_{1}(\tau)\bar{T},
\frac{d\bar{R}}{d\tau} = -\bar{a}_{4} \frac{\bar{L}\bar{R}}{\bar{K}_{R} + \bar{R}} - \bar{a}_{5}\bar{L}\bar{R} + \bar{a}_{6}\bar{C},
\frac{d\bar{C}}{d\tau} = -\bar{a}_{1} \frac{\bar{C}\bar{H}}{\bar{K}_{H} + \bar{H}} - \bar{a}_{2}\bar{C}\bar{H} + \bar{a}_{3}\bar{T} + \bar{a}_{4} \frac{\bar{L}\bar{R}}{\bar{K}_{R} + \bar{R}} + \bar{a}_{5}\bar{L}\bar{R} - \bar{a}_{6}\bar{C} - \bar{\beta}_{2}\bar{u}_{2}(\tau)\bar{C},
\frac{d\bar{L}}{d\tau} = -\bar{a}_{7}\bar{R}\bar{L} + \bar{a}_{8}\bar{C} + \bar{a}_{9}\bar{L} - \bar{a}_{10}\bar{L},
\bar{H}(0) = \bar{H}_{0}, \ \bar{T}(0) = \bar{T}_{0}, \ \bar{R}(0) = \bar{R}_{0}, \ \bar{C}(0) = \bar{C}_{0}, \ \bar{L}(0) = \bar{L}_{0}.$$
(1)

The unknown patient-specific parameters that need to be determined is the parameter vector $\tilde{\boldsymbol{\theta}} = (\bar{a}_1, \dots, \bar{a}_{10})$. The functions \bar{u}_i i=1,2 represent dosages of Trastuzumab and Bevacizumab [10], with efficacy rates $\bar{\beta}_1, \bar{\beta}_2$, respectively. The rationale behind the modeling of the combination doses is as follows: Trastuzumab binds to the extracellular domain of the HER2 receptor and inhibits HER2 homodimerization. This, in turn, prevents HER2-mediated signaling [22]. For this reason, we represent the action of Trastuzumab through a mass action law on the EGF:EGFR:HER2 complex. On the other hand, Bevacizumab attaches to the VEGF protein and blocks its growth [29]. Due to the fact that the VEGF and EGFR pathways share common downstream signaling pathways and EGF ligand is one of the many growth factors that drive VEGF expression [11, 23], we model the action of Bevacizumab by a mass action law on the EGF:EGFR complex.

For stabilization and scalability of the numerical algorithms, we non-dimensionalize the above ODE system using the following non-dimensionalized state and time variables, and parameters

$$H = d_{1}\bar{H}, \ T = d_{1}\bar{T}, \ R = d_{1}\bar{R}, \ C = d_{1}\bar{C}, \ L = d_{2}\bar{L}, \ t = d_{3}\tau,$$

$$a_{1} = \frac{\bar{a}_{1}}{d_{3}}, \ a_{2} = \frac{\bar{a}_{2}}{d_{1}d_{3}}, \ a_{3} = \frac{\bar{a}_{3}}{d_{3}}, \ a_{4} = \frac{d_{1}\bar{a}_{4}}{d_{2}d_{3}}, \ a_{5} = \frac{d_{1}\bar{a}_{5}}{d_{3}},$$

$$a_{6} = \frac{\bar{a}_{6}}{d_{3}}, \ a_{7} = \frac{\bar{a}_{7}}{d_{1}d_{3}}, \ a_{8} = \frac{d_{2}\bar{a}_{8}}{d_{2}d_{3}}, \ a_{9} = \frac{\bar{a}_{9}}{d_{3}}, \ a_{10} = \frac{\bar{a}_{10}}{d_{3}}$$

$$(2)$$

The transformed non-dimensionless ODE system is given as follows

$$\frac{dH}{dt} = -a_1 \frac{CH}{K_H + H} - a_2 CH + a_3 T,$$

$$\frac{dT}{dt} = a_1 \frac{CH}{K_H + H} + a_2 CH - a_3 T - \beta_1 u_1(t) T,$$

$$\frac{dR}{dt} = -a_4 \frac{LR}{K_R + R} - a_5 LR + a_6 C,$$

$$\frac{dC}{dt} = -a_1 \frac{CH}{K_H + H} - a_2 CH + a_3 T + a_4 \frac{LR}{K_R + R} + a_5 LR - a_6 C - \beta_2 u_2(t) C,$$

$$\frac{dL}{dt} = -a_7 RL + a_8 C + a_9 L - a_{10} L,$$

$$H(0) = H_0, \ T(0) = T_0, \ R(0) = R_0, \ C(0) = C_0, \ L(0) = L_0,$$
(3)

where $t \in (0, T_f)$. The system of ODEs given in (3) can be written in a compact form as follows

$$\frac{d\mathbf{X}}{dt} = \mathbf{F}(\mathbf{X}, \boldsymbol{\theta}, \mathbf{U}),
\mathbf{X}(0) = \mathbf{X}_0,$$
(4)

where $\boldsymbol{X}(t) = (H(t), T(t), RT(t), C(t), L(t))^T$, $\boldsymbol{\theta} = (a_1, \dots, a_{10}) \in T_{ad} = \{\boldsymbol{\theta} \in \mathbb{R}^{10} : 0 \leq \boldsymbol{\theta}_i \leq M_i\}$ and $\boldsymbol{U} = (u_1, u_2) \in U_{ad} = U_{ad}^1 \times U_{ad}^2$, with $U_{ad}^i = \{u \in L^2(0, T_f) : 0 \leq u(t) \leq D_i, \forall t \in (0, T_f)\}$

2.1 Optimal control algorithm for combination therapies

Here we describe a three-step algorithm for obtaining the optimal combination therapies.

1. We first estimate the patient specific unknown parameter vector $\boldsymbol{\theta}$, given the values of \boldsymbol{X} at specific time instants t_1, \dots, t_N as \boldsymbol{X}_i^d , $i = 1, \dots, N$. Note that data for some components of \boldsymbol{X} might not be specified, and data can be noisy. We solve the following optimization problem

$$\boldsymbol{\theta}^* = \underset{\boldsymbol{\theta} \in T_{ad}}{\operatorname{arg\,min}} J_1(\boldsymbol{X}, \boldsymbol{\theta}) := \frac{\alpha}{2} \int_0^{T_f} (\boldsymbol{X}(t) - \boldsymbol{X}^d(t))^2 \, dx + \frac{\gamma}{2} \|\boldsymbol{\theta}\|_{l^2}^2, \tag{5}$$

subject to the QSP system (3) with U = 0, where $X^d(t)$ is the data function formed by interpolating the patient data $X_i^d(t)$. The first term in the expression of J_1 in (5) is the

standard least squares fitting term. The second term is a l^2 regularization term for $\boldsymbol{\theta}$. Such a regularization term prevents any one (or multiple) of the parameter values in $\boldsymbol{\theta}$ from getting too far out of control.

- 2. In the next step, we determine the subset of the optimal parameter set θ^* that is sensitive with respect to the EGF:EGFR complex C. This will be achieved through a global uncertainty and sensitivity analysis using the Latin hypercube sampling-partial rank correlation coefficient method (LHS-PRCC), as described in Section 4.1.
- 3. Using the information of the sensitive parameters from the previous step, we now decide on the type of drugs to be chosen, and the number of different drugs to be used, represented by the number of $\beta_i \neq 0$. We then formulate a second optimization problem as follows:

$$\min_{u_i \in U_{ad}^i, \beta_i \neq 0} J_2(u_i, f) := \frac{\nu_1}{2} (C(T_f) - C^*)^2 + \frac{\nu_2}{2} (T(T_f) - T^*)^2 + \sum_{i=1, \beta_i \neq 0}^2 \frac{\eta_i}{2} \int_0^{T_f} u_i^2(t) \ dt, \quad (6)$$

subject to the QSP system (3), where C^* , T^* are targets EGF:EGFR and EGF:EGFR:HER2 complexes. The first two terms in the expression of J_2 in (6) serve as the target of the drugs for driving C, T to the desired target values C^*, T^* at the final time T_f . The choice of such terms in the functional is motivated by the scenario where variable dosage treatment is administered on a sequence of days so as to achieve a desired target on a monitoring day (T_f) , which is similar to a treatment regime like an antibiotic. The second term is a l^2 regularization term for u_i , which controls, possibly, large dosages of the drugs while achieving the desired targets.

At the end of Step 3, we not only obtain the types of drugs that can be used for treatment but also the optimal drug concentration and the dosage profile over time.

3 Theory of the optimal control problem

In this section we describe some theoretical properties of the ODE system (4). We first begin with the positivity of the solutions of (4).

Lemma 3.1. The solutions of (4) are non-negative in the sense that if $X_0 \ge 0$, we have $X(t) \ge 0$ for all $t \in [0, T_f]$.

Proof. We can write (4) in a productive-destructive form as follows:

$$\frac{d\mathbf{X}}{dt} = \mathbf{P}(\mathbf{X}, \boldsymbol{\theta}) - \mathbf{D}(\mathbf{X}, \boldsymbol{\theta}, \mathbf{U})\mathbf{X},\tag{7}$$

where P, D are positive, i.e., if $X, \theta \ge 0$, we have $P, D \ge 0$, componentwise. Consider the integrating factor vector $I = \exp(\int D \, dt)$. The (7) can be rewritten as

$$\frac{d(\mathbf{IX})}{dt} = \mathbf{P}(\mathbf{I}, \boldsymbol{\theta}). \tag{8}$$

Since, $X_0 \ge 0$, we have $IX_0 \ge 0$. Thus, (8) gives us that $IX(t) \ge 0$ for all $t \in [0, T_f]$. Since, I > 0, we have that $X(t) \ge 0$ for all $t \in [0, T_f]$.

We next prove some stability estimate for the solution of (4).

Lemma 3.2. A solution $\mathbf{X} = (H, T, R, C, L)$ of (4) satisfies the following stability estimate

$$H(t) + T(t) \le H_0 + T_0,$$

$$R(t) + C(t) + T(t) \le R_0 + C_0 + T_0,$$

$$L(t) \le \exp(a_9 T_f) (L_0 + K(\theta, \mathbf{X}_0)).$$
(9)

Proof. From (4), we note the following:

$$\frac{d(H+T)}{dt} = -\beta_1 u_1(t)T \le 0,$$

$$\frac{d(R+C+T)}{dt} = -\beta_2 u_2(t)T \le 0,$$

$$\frac{dL}{dt} \le a_8 C(t) + a_9 L.$$

A simple application of Gronwall's inequality gives the desired result.

Lemma 3.2 gives us that a solution X of (4) is bounded. We now state and prove the existence and uniqueness of solutions of (4).

Theorem 3.1. Given $U \in U_{ad}$, there exists an unique solution X of (4) in $(H^1(0,T_f))^5$.

Proof. Since $U \in U_{ad}$, U is bounded. From Lemma 3.2, we have that X is bounded. These two results yield that F satisfies the following conditions:

- 1. F is continuous with respect to X.
- 2. \mathbf{F} is measurable with respect to t.
- 3. \boldsymbol{F} is bounded.
- 4. The derivative of F with respect to X is also bounded.

Thus, F satisfies the Caratheodory's conditions, which gives the existence and uniqueness of a solution $X \in (H^1(0,T_f))^5$ of (4).

The aforementioned results give that the mapping $\Lambda: T_{ad} \times U_{ad} \to H^1(0, T_f)$, $(\boldsymbol{\theta}, \boldsymbol{U}) \to \boldsymbol{X} = \Lambda(\boldsymbol{\theta}, \boldsymbol{U})$ is continuous. Further, using similar arguments as in [1, 31, 32], it can be shown that this mapping is also Fréchet differentiable. We now discuss some properties of the cost functionals J_1, J_2 given in (5) and (6).

Proposition 1. The objective functionals J_1 , J_2 , given in (5) and (6), are sequentially weakly lower semi-continuous (w.l.s.c.), bounded from below, coercive on T_{ad} , U_{ad} . respectively, and are Fréchet differentiable.

With this preparation, we are now ready to state and prove the existence of the optimal parameter set θ^* and the optimal drug dosage concentration vector U^* in the following theorem.

Theorem 3.2. Let J_1, J_2 be given as in (5) and (6). Then, there exists pairs $(\boldsymbol{X}_1^*, \boldsymbol{\theta}^*) \in H^1(0, T_f) \times T_{ad}$ and $(\boldsymbol{X}_2^*, \boldsymbol{U}^*) \in (H^1(0, T_f))^5 \times U_{ad}$ such that $\boldsymbol{X}_1^*, \boldsymbol{X}_2^*$ are solutions of (4), and $\boldsymbol{\theta}^*, \boldsymbol{U}^*$ minimize J_1, J_2 in T_{ad}, U_{ad} , respectively.

Proof. We first prove the existence of minimizer of J_1 in (5). Since J_1 is bounded below, there exists a minimizing sequence $(\boldsymbol{\theta}^m) \in T_{ad}$. Since $T_{ad} \subset \mathbb{R}^{10}$, and J_1 is sequentially w.l.s.c. as well as coercive in T_{ad} , this sequence is bounded. Therefore, it contains a convergent subsequence $(\boldsymbol{\theta}^{m_l})$ in T_{ad} such that $\boldsymbol{\theta}^{m_l} \to \boldsymbol{\theta}^*$. Correspondingly, the sequence (\boldsymbol{X}^{m_l}) , where $\boldsymbol{X}^{m_l} = \Lambda(\boldsymbol{\theta}^{m_l}, 0)$, is bounded in $(L^2(0, T_f))^5$ while the sequence of the time derivatives, $(\partial_t \boldsymbol{X}^{m_l})$, is bounded in $(L^2(0, T_f))^5$ by Lemma 3.2 and Theorem 3.1. Therefore, both the sequences converge weakly to \boldsymbol{X}_1^* and $\partial_t \boldsymbol{X}_1^*$, respectively. From the above discussion, we obtain weak convergence of the sequence $(\boldsymbol{F}(\boldsymbol{X}^{m_k}, \boldsymbol{\theta}^{m_k}, 0))$ in $(L^2(0, T_f))^5$. It now follows that $\boldsymbol{X}_1^* = \Lambda(\boldsymbol{\theta}^*, 0)$, and the pair $(\boldsymbol{X}_1^*, \boldsymbol{\theta}^*)$ minimizes J_1 .

For proving existence of a minimizer of J_2 , given in (6), we can follow the same arguments as above, due to the fact that U_{ad} is a closed subspace of a Hilbert space and J_2 is coercive in U_{ad} , which yields a weakly convergent subsequence (u_{m_l}) of a minimizing sequence (\boldsymbol{U}_m) for J_2 . The compactness result of Aubin-Lions [20] yields strong convergence of a subsequence (\boldsymbol{X}^{m_k}) of a sequence $(\boldsymbol{X}^{m_l} = \Lambda(\boldsymbol{\theta}^*, \boldsymbol{U}_{m_l}))$ in $(L^2(0, T_f))^5$. From the above discussion, we obtain weak convergence of the sequence $(\boldsymbol{F}(\boldsymbol{X}^{m_k}, \boldsymbol{\theta}^*, \boldsymbol{U}_{m_k}))$ in $(L^2(0, T_f))^5$. It now follows that $\boldsymbol{X}_2^* = \Lambda(\boldsymbol{\theta}^*, \boldsymbol{U}^*)$, and the pair $(\boldsymbol{X}_2^*, \boldsymbol{U}^*)$ minimizes J_2 .

The Frechét differentiability of J_1 , J_2 gives rise to the first order necessary optimality conditions as follows: For the minimization problem (5), the optimality system is given as

$$\frac{dH}{dt} = -a_1 \frac{CH}{K_H + H} - a_2 CH + a_3 T,$$

$$\frac{dT}{dt} = a_1 \frac{CH}{K_H + H} + a_2 CH - a_3 T,$$

$$\frac{dR}{dt} = -a_4 \frac{LR}{K_R + R} - a_5 LR + a_6 C,$$

$$\frac{dC}{dt} = -a_1 \frac{CH}{K_H + H} - a_2 CH + a_3 T + a_4 \frac{LR}{K_R + R} + a_5 LR - a_6 C,$$

$$\frac{dL}{dt} = -a_7 RL + a_8 C + a_9 L - a_{10} L,$$

$$H(0) = H_0, T(0) = T_0, R(0) = R_0, C(0) = C_0, L(0) = L_0,$$
(FOR1)

$$\begin{split} &-\frac{d\widetilde{H}}{dt} = a_1 C K_H \frac{\widetilde{T} - \widetilde{H} - \widetilde{C}}{(K_H + H)^2} + a_2 C (\widetilde{T} - \widetilde{H} - \widetilde{C}) - \alpha (H - H^d), \\ &-\frac{d\widetilde{T}}{dt} = a_3 (\widetilde{C} + \widetilde{H} - \widetilde{T}) - \alpha (T - T^d), \\ &-\frac{d\widetilde{R}}{dt} = a_4 L K_R \frac{\widetilde{C} - \widetilde{R}}{(K_R + R)^2} + a_5 L (\widetilde{C} - \widetilde{L}) - \alpha (R - R^d), \\ &-\frac{d\widetilde{C}}{dt} = a_1 H \frac{\widetilde{T} - \widetilde{H} - \widetilde{C}}{(K_H + H)} + a_2 H (\widetilde{T} - \widetilde{H} - \widetilde{C}) - a_6 \widetilde{C} + a_8 \widetilde{L} - \alpha (C - C^d), \\ &-\frac{d\widetilde{L}}{dt} = a_4 R \frac{\widetilde{C} - \widetilde{R}}{K_R + R} + a_5 R \widetilde{C} - a_7 R \widetilde{L} + a_9 \widetilde{L} - a_{10} \widetilde{L} - \alpha (L - L^d), \\ \widetilde{H}(T_f) = 0, \ \widetilde{T}(T_f) = 0, \ \widetilde{R}(T_f) = 0, \ \widetilde{C}(T_f) = 0, \ \widetilde{L}(T_f) = 0, \\ &\left(\gamma a_1 + C H \frac{\widetilde{H} + \widetilde{C} - \widetilde{T}}{K_H + H}\right) (\widetilde{a}_1 - a_1) \geq 0, \\ &\left(\gamma a_3 + T (\widetilde{T} - \widetilde{H} - \widetilde{C})\right) (\widetilde{a}_3 - a_3) \geq 0, \\ &\left(\gamma a_3 + L R \frac{\widetilde{R} - \widetilde{C}}{K_R + R}\right) (\widetilde{a}_4 - a_4) \geq 0, \\ &\left(\gamma a_5 + L R (\widetilde{R} - \widetilde{C})\right) (\widetilde{a}_5 - a_5) \geq 0, \\ &\left(\gamma a_6 + C (\widetilde{C} - w R)\right) (\widetilde{a}_6 - a_6) \geq 0, \\ &\left(\gamma a_8 - C \widetilde{L}\right) (\widetilde{a}_8 - a_8) \geq 0, \\ &\left(\gamma a_9 - L \widetilde{L}\right) (\widetilde{a}_9 - a_9) \geq 0, \\ &\left(\gamma a_{10} + L \widetilde{L}\right) (\widetilde{a}_{10} - a_{10}) \geq 0, \end{split}$$

for all $\tilde{\boldsymbol{\theta}} = (\tilde{a}_1, \dots, \tilde{a}_{10}) \in T_{ad}$. For the minimization problem (6), the optimality system is given

 $\frac{dH}{dt} = -a_1 \frac{CH}{K_H + H} - a_2 CH + a_3 T,$ $\frac{dT}{dt} = a_1 \frac{CH}{K_{II} + H} + a_2 CH - a_3 T - \beta_1 u_1(t) T,$ $\frac{dR}{dt} = -a_4 \frac{LR}{K_B + R} - a_5 LR + a_6 C,$ (FOR2) $\frac{dC}{dt} = -a_1 \frac{CH}{K_{II} + H} - a_2 CH + a_3 T + a_4 \frac{LR}{K_{IP} + R} + a_5 LR - a_6 C - \beta_2 u_2(t) C,$ $\frac{dL}{dL} = -a_7 R L + a_8 C + a_9 L - a_{10} L,$ $H(0) = H_0, T(0) = T_0, R(0) = R_0, C(0) = C_0, L(0) = L_0,$ $-\frac{d\widetilde{H}}{dt} = a_1 C K_H \frac{\widetilde{T} - \widetilde{H} - \widetilde{C}}{(K_{TT} + H)^2} + a_2 C (\widetilde{T} - \widetilde{H} - \widetilde{C}),$ $-\frac{dT}{dt} = a_3(\widetilde{C} + \widetilde{H} - \widetilde{T}) - \beta_1 u_1(t)\widetilde{T} - \nu_1(T - T^*),$ $-\frac{d\widetilde{R}}{dt} = a_4 L K_R \frac{\widetilde{C} - \widetilde{R}}{(K_D + R)^2} + a_5 L (\widetilde{C} - \widetilde{L}),$ (ADJ2) $-\frac{d\widetilde{C}}{dt} = a_1 H \frac{\widetilde{T} - \widetilde{H} - \widetilde{C}}{(K_{II} + H)} + a_2 H (\widetilde{T} - \widetilde{H} - \widetilde{C}) - a_6 \widetilde{C} + a_8 \widetilde{L} - \beta_2 u_2(t) \widetilde{C} - \nu_2 (C - C^*),$ $-\frac{d\widetilde{L}}{dt} = a_4 R \frac{\widetilde{C} - \widetilde{R}}{K_D + R} + a_5 R \widetilde{C} - a_7 R \widetilde{L} + a_9 \widetilde{L} - a_{10} \widetilde{L},$ $\widetilde{H}(T_f) = 0, \ \widetilde{T}(T_f) = 0, \ \widetilde{R}(T_f) = 0, \ \widetilde{C}(T_f) = 0, \ \widetilde{L}(T_f) = 0.$ $\langle n_1 u_1(t) + \beta_1 T(t) \widetilde{T}(t), \widetilde{u}_1(t) - u_1(t) \rangle_{T^2(0,T_2)} > 0.$ (OPT2)

for all $\tilde{\boldsymbol{U}} = (\tilde{u}_1, \tilde{u}_2) \in U_{ad}$.

4 Numerical discretization schemes for solving the optimality system and sensitivity analysis

 $\langle \eta_2 u_2(t) + \beta_2 C(t) \widetilde{C}(t), \widetilde{u}_2(t) - u_2(t) \rangle_{L^2(0,T_c)} > 0,$

In this section, we describe the numerical schemes for solving the optimality system (FOR1)-(OPT1) and (FOR2)-(OPT2). We first divide the interval $(0, T_f)$ into N_t subintervals and form the mesh

$$M^h = \{t_k : t_k = kh, \ 0 \le k \le N_t\},\$$

where $h = T_f/N_t$. To solve the forward and the adjoint equations, we use the non-standard finite difference (NSFD) schemes. NSFD schemes are a class of finite difference schemes that uses a

modified denominator function in the discretization of the time derivative in order to achieve elementary stability. Traditionally, positive Euler-based NSFD methods are first order. But very recently, a class of second-order, elementary stable positive Euler-based modified NSFD methods were devised for solving ODE systems. The starting point is to note that both the forward ODE system (4) and the corresponding adjoint ODE systems (ADJ1), (ADJ2), after using a transformation of variables to rewrite them as an initial value problem, can be written in the generic form as:

$$\frac{d\mathbf{Y}}{dt} = \mathbf{G}(\mathbf{Y}, \boldsymbol{\theta}, \mathbf{U}), \ \mathbf{Y}(0) = \mathbf{Y}^{0}.$$
 (10)

The corresponding NSFD discretization can be described as follows: Let $\mathbf{Y}^k \approx \mathbf{Y}(t_k)$, be the numerical solution of (10) at the grid point t_k . Then starting with \mathbf{Y}^0 at the initial time, \mathbf{Y}^k can be obtained using the NSFD numerical scheme

$$\frac{\boldsymbol{Y}_{i}^{k+1} - \boldsymbol{Y}_{i}^{k}}{\phi_{i}(h, \boldsymbol{Y})} = \begin{cases}
\boldsymbol{G}(\boldsymbol{Y}_{k}, \boldsymbol{\theta}, \boldsymbol{U}(t_{k})), & \text{if } \boldsymbol{G}(\boldsymbol{Y}_{k}, \boldsymbol{\theta}, \boldsymbol{U}(t_{k})) \geq 0 \\
\frac{\boldsymbol{Y}_{i}^{k+1}}{\boldsymbol{Y}_{i}^{k}} \boldsymbol{G}(\boldsymbol{Y}_{k}, \boldsymbol{\theta}, \boldsymbol{U}(t_{k})), & \text{if } \boldsymbol{G}(\boldsymbol{Y}_{k}, \boldsymbol{\theta}, \boldsymbol{U}(t_{k})) < 0
\end{cases}$$
(11)

for $k = 0, ..., N_t - 1$, i = 1, ..., 5, where $\phi_i(h, \mathbf{Y}) = \frac{1 - \exp(-q_i(\mathbf{Y})h)}{q_i(\mathbf{Y})}$, with

$$q_{i}(\mathbf{Y}) = \begin{cases} -\frac{\langle \nabla_{\mathbf{Y}} \mathbf{G}_{i}(\mathbf{Y}), \mathbf{G}(\mathbf{Y}) \rangle}{\mathbf{G}_{i}(\mathbf{Y})}, & \mathbf{G}_{i}(\mathbf{Y}) \geq 0\\ \frac{2\mathbf{G}_{i}(\mathbf{Y})}{\mathbf{Y}_{i}} - \frac{\langle \nabla_{\mathbf{Y}} \mathbf{G}_{i}(\mathbf{Y}), \mathbf{G}(\mathbf{Y}) \rangle}{\mathbf{G}_{i}(\mathbf{Y})}, & \mathbf{G}_{i}(\mathbf{Y}) < 0 \end{cases}$$
(12)

The NSFD scheme (11) is positive, elementary stable, and second order accurate.

For solving the optimization problems (5) and (6), we use a projected non-linear conjugate gradient (NCG) scheme. NCG schemes are a class of non-linear optimization schemes for solving optimization problems with the objective functional nonlinear yet differentiable with respect to the optimization variables. Such a scheme has been used to solve several finite and infinite dimensional optimization problems. It has been demonstrated to provide robust and accurate solutions of the optimality system, even for finite dimensional optimization problems. For non-linear optimization schemes involving non-differentiable objective functionals, one can use proximal methods, semi-smooth Newton schemes, or gradient free schemes based on the Pontryagin's maximum principle. We describe below the NCG scheme for solving the minimization problems (5) and (6). For this purpose, we generically denote the reduced functional corresponding to either of the minimization problems as \hat{J} , and the associated optimization variable as P. Starting with the initial guess P_0 , we compute the first descent direction as

$$d_0 = -g_0 := \nabla_{\mathbf{P}} \hat{J}(\mathbf{P}_0),$$

where $\nabla_{\mathbf{P}}\hat{J}$ is given by (OPT1) or (OPT2). We then obtain the search directions recursively as follows

$$d_{k+1} = -g_{k+1} + \beta_k d_k, (13)$$

where $g_k = \nabla \hat{J}(u_k)$, $k = 0, 1, \ldots$ The parameter β_k is chosen according to the formula of Hager-Zhang given by

$$\beta_k^{HG} = \frac{1}{d_k^T y_k} \left(y_k - 2d_k \frac{\|y_k\|_{l^2}^2}{d_k^T y_k} \right)^T g_{k+1}, \tag{14}$$

where $y_k = g_{k+1} - g_k$. Next, a conjugate gradient descent step is used to compute the new optimization variable iterate

$$P_{k+1} = P_k + \alpha_k \, d_k,\tag{15}$$

where k is an index of the iteration step and $\alpha_k > 0$ is a steplength obtained using a backtracking line search algorithm. In this update, we use the following Armijo condition of sufficient decrease of \hat{J} for the backtracking line search

$$\hat{J}(\mathbf{P}_k + \alpha_k d_k) \le \hat{J}(\mathbf{P}_k) + \delta \alpha_k \langle \nabla_{\mathbf{P}} \hat{J}(\mathbf{P}_k), d_k \rangle_{L^2}, \tag{16}$$

where $0 < \delta < 1/2$ and the scalar product $\langle u, v \rangle_{L^2}$ is the discrete l^2 inner product in \mathbb{R}^{10} for the minimization problem (5), and represents the standard $L^2([0,T])^2$ inner product for the minimization problem (6). The gradient update step is finally combined with the following projection step to ensure that the iterates stay in the admissible sets.

$$\boldsymbol{P}_{k+1} = P_U \left[\boldsymbol{P}_k + \alpha_k \, d_k \right], \tag{17}$$

where

$$P_U[\mathbf{P}] = (\max\{0, \min\{N_i, \mathbf{P}_i\}\}), \ \forall i = 1, \dots, s),$$

with $U = T_{ad}$ or U_{ad} , s = 10 or 2 and $N_i = M_i$ or D_i , corresponding to the minimization problems (5) and (6), respectively. The following algorithm summarizes the projected NCG scheme:

Algorithm 4.1 (Projected NCG Scheme).

- 1. Input: initial approx. \mathbf{P}_0 . Evaluate $d_0 = -\nabla_{\mathbf{P}} \hat{J}(\mathbf{P}_0)$, index k = 0, maximum $k = k_{max}$, tolerance =tol.
- 2. While $(k < k_{max})$ do
- 3. Set $P_{k+1} = P_U[P_k + \alpha_k d_k]$, where α_k is obtained using a line-search algorithm.
- 4. Compute $g_{k+1} = \nabla_{\mathbf{P}} \hat{J}(\mathbf{P}_{k+1})$.
- 5. Compute β_k^{HG} using (14).
- 6. Set $d_{k+1} = -g_{k+1} + \beta_k^{HG} d_k$.
- 7. If $\|\mathbf{P}_{k+1} \mathbf{P}_k\|_{l^2} < tol$, terminate.
- 8. Set k = k + 1.
- 9. End while.

4.1 Global sensitivity analysis of optimal parameter set

After obtaining the optimal parameter set, we next want to determine the most sensitive parameters with respect to the EGF:EGFR complex C. The reason for this is because patient-specific parameters can vary due to uncertainties in the data, and, thus, they can be considered as random variables. Furthermore, it is important to understand which of these parameters affect the huge change in C and this will help us determine what kind of drugs can be chosen to control the cancer.

Traditional sensitivity analysis of parameters are carried out using a local approach where the sensitivity of one parameter is studied separately by keeping rest of the parameters fixed at their baseline values. However, this may not reflect an accurate measure of the sensitivity of each parameter due to the absence of incorporating simultaneous effects of other parameters [12]. Thus, we employ a global sensitivity analysis that allows identification of the effects all the parameters, simultaneously. For this purpose, we will use the combined Latin hypercube sampling (LHS) method and partial rank correlation coefficient (PRCC) method (LHS-PRCC) [21]. In context of parameter sensitivity in mathematical models of cancer, such a technique was successfully applied in [33] for identifying the treatment types in colon cancer. To the best of our knowledge, this technique is being applied for the first time in context of developing optimal treatments for controlling pathways in esophageal cancer. The sensitivity of the parameters in (3) is carried out with respect to the outcome of interest, which is the sum of C and T at the final time T_f . The null hypothesis for the corresponding p-values for each parameter is that there is no significant correlation between the parameter and the outcome of interest. Any parameter having p-values greater than 0.05 implies that the null hypothesis is true and, thus, the corresponding parameter does not affect the change in C and T. We refer to [33] for details of the LHS-PRCC algorithm for sensitivity analysis of the optimal parameter set.

5 Numerical results

We now present numerical results of the proposed optimal control framework in Section 2. For this purpose, we choose our non-dimensionalized scaling parameters d_1, d_2, d_3 , as given in (2) as $d_1 = 10^{-5}, d_2 = 10^3, d_3 = 10^{-2}$. With the original time interval as (0, 100) hours, this transformation yields the final time $T_f = 1$. We divide the time interval (0, 1) into 1000 equally-spaced subintervals.

For test case 1, the patient data is generated as follows: We first simulate the following reduced ODE system for $t \in (0,1)$ on a grid of 501 equally spaced points

$$\frac{dC}{dt} = k_f(R_N - C)L - k_r C, \ C(0) = C_0$$

$$\frac{dL}{dt} = -c_L k_f(R_N - C)L + c_L k_r C + S_L - \lambda_d L, \ L(0) = L_0,$$
(18)

with parameter values $k_f = 0.297$, $k_r = 0.224$, $\lambda_d = 1$, $S_L = 0.5$, $R_N = 10$, $c_L = 2.5$, and initial conditions $C_0 = 1.7$, L(0) = 1.8. This reduced model is derived from equations (8a)-(8c) in [6], in context of EGFR signaling in breast cancer cell, assuming non-information of the

HER2 complex formation dynamics. The motivation of such an assumption is to use partial information about the EGF:EGFR complex C formation dynamics to replicate some type of possible heterogeneity in context of an EC cell, since there is a lack of real data about the complexes for an actual EC cell. To the solution (C(t), L(t)) obtained, we then add 10% additive Gaussian noise. This gives us our data C^d , L^d . We also provide initial conditions for the remaining variables as $H_0 = 5.6$, $T_0 = 5.23$, $R_0 = 3.07$. We first solve the parameter estimation minimization problem (5) using the PNCG method, with weights in the functional J_1 as $\alpha = 1.0$, $\gamma = 0.01$. With the parameter estimates, the ODE system (3) is simulated with the aforementioned initial conditions. The plots of the obtained C, L and the data C^d , L^d are shown in Figure 1. We see that the simulated C, L resembles the mean trajectory.

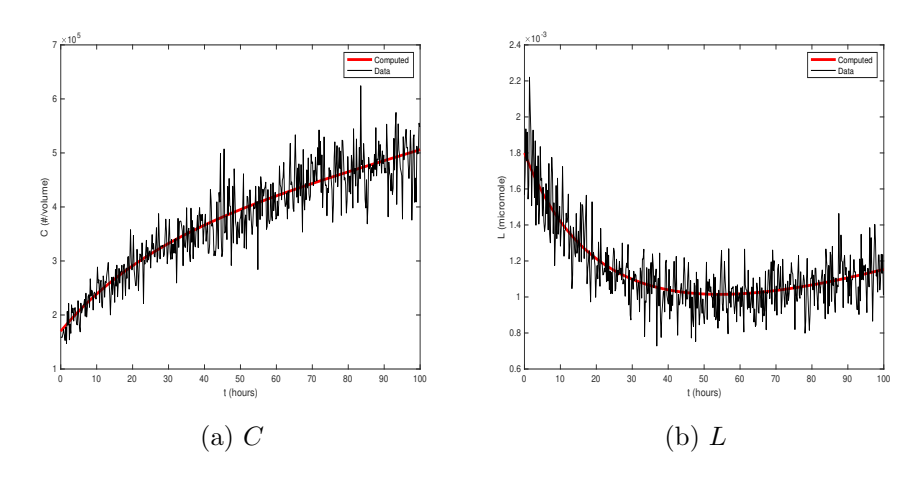


Figure 1: Test Case 1: Plots of the data and the fitted curves of C, L after the parameter estimation

We next perform a sensitivity analysis of the obtained parameter set with respect to the sum of C, T at the final time $T_f = 1.0$. For this purpose, we assume each parameter to follow a Weibull distribution [25, 26] and consider the number of equiprobable intervals, M, to be 100. The p-values are given in Table 1.

Parameter	p− value
a_1	0.0075319
a_2	2.7492e-47
a_3	0.019495
a_4	2.05e-05
a_5	4.3642e-82
a_6	0.018705
a_7	1.289e-09
a_8	3.3458e-230
a_9	0.0088942
a_{10}	7.0862e-65

Table 1: Test case 1: p-values for the optimal parameter set θ^*

.

We note that in the ODE system (3) the drug dosages u_1, u_2 have been incorporated with interaction terms similar to the uncoupling terms with rates a_3, a_6 . We now note from the p-values in Table 1 that both the parameters a_3, a_6 have p-values less than 0.05, which means they are significantly sensitive in the change of C, T. Thus, the combination drug is required to bring down the values of C, T, and so $\beta_1, \beta_2 \neq 0$. In this test case, β_1, β_2 are chosen to be 0.7. We now solve the second optimal control problem (6) to obtain the optimal dosages u_1, u_2 . For this purpose, we start the observation at the non-dimensional time t = 0.33 (corresponding to the actual time of 33 hours). Our aim is to drive the non-dimensional values of C, T to 2 (corresponding to the actual values 200,000) after treatment till non-dimensional time t = 1.3 (corresponding to the actual time of 133 hours). We choose the values of the weights in the functional J_2 as $\nu_1 = 1.0, \nu_2 = 1.0, \eta_1 = 0.001, \eta_2 = 0.001$. We observe the evolution of C, T with and without the treatments, as shown in Figure 2.

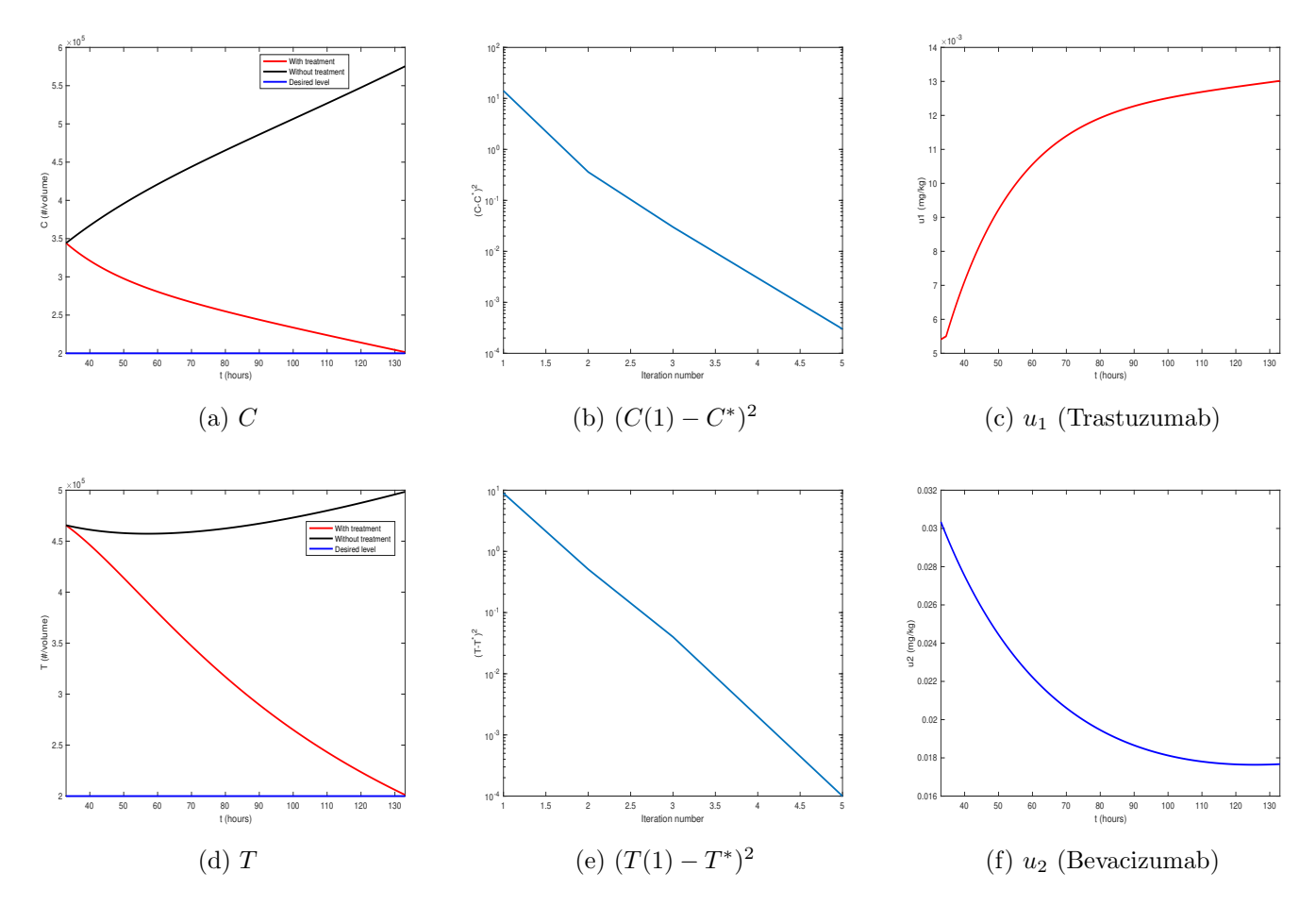


Figure 2: Test Case 1: Plots of the dosages and evolution of C, T with and without treatments.

We note that without treatment, the profiles of C, T (in black) increase, leading to prominence of the EC cell. However, with the combination treatment of Trastuzumab and Bevacizumab, we have achieve the goal to drive the values of C, T to or below the desired level that renders the EC cell ineffective, thus demonstrating the effectiveneness of our framework in obtaining personalized therapies. We also note from Figure 2(b) and (e), the evolution of $(C(T_f) - C^*)^2, (T(T_f) - T^*)^2$ during the optimal control process against the iterate number. We observe a monotonic decrease till convergence is achieved.

In the second test case, we simulate the ODE system (18) with parameter values $k_f = 0.297$, $k_r = 0.224$, $\lambda_d = 1$, $S_L = 0.5$, $R_N = 10$, $c_L = 1.8$, and initial conditions $C_0 = 1.7$, L(0) = 1.8. To the solution (C(t), L(t)) obtained, we then add 10% additive Gaussian noise. This gives us our data C^d , L^d . We also provide initial conditions for the remaining variables as $H_0 = 4.6$, $T_0 = 4.23$, $R_0 = 4.07$. We again solve the parameter estimation problem (5), with weights in the functional J_1 as $\alpha = 1.0$, $\gamma = 0.01$. and check for the fits of C, L, as shown in Figure 3.

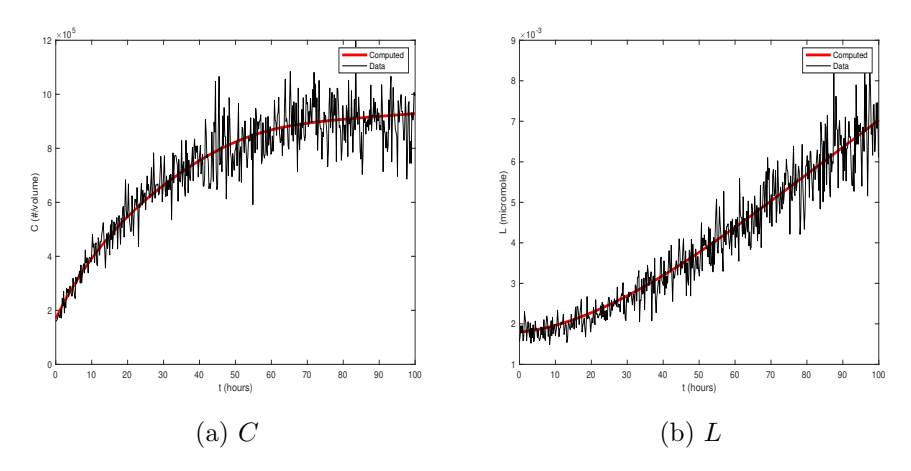


Figure 3: Test Case 2: Plots of the data and the fitted curves of C, L after the parameter estimation

We again perform a sensitivity analysis of the obtained parameter set. The p-values are shown in Table 2.

Parameter	<i>p</i> − value
a_1	0.11127
a_2	4.6699e-05
a_3	0.71739
a_4	0.44192
a_5	5.2e-80
a_6	0.0091312
a_7	0.5721
a_8	5.7334e-56
a_9	0.5592
a_{10}	5.3506e-09

Table 2: Test case 2: p-values for the optimal parameter set θ^*

.

From Table 2, we now see that the parameter a_3 has a p-value greater than 0.05 whereas a_6 still has a p-value less than 0.05. Thus, a_3 is not sensitive anymore to the change of C, T and so the drug Trastuzumab, represented by u_1 will not be effective for control anymore. We, thus, set $\beta_1 = 0$ and $\beta_2 = 0.7$ and proceed to solve the optimal control problem 6 to drive the non-dimensional value of C to 2 and the non-dimensional value of C to 0.5 at the final non-dimensional time C to 1.33. We choose the values of the weights in the functional C as C are shown in Figure 4.

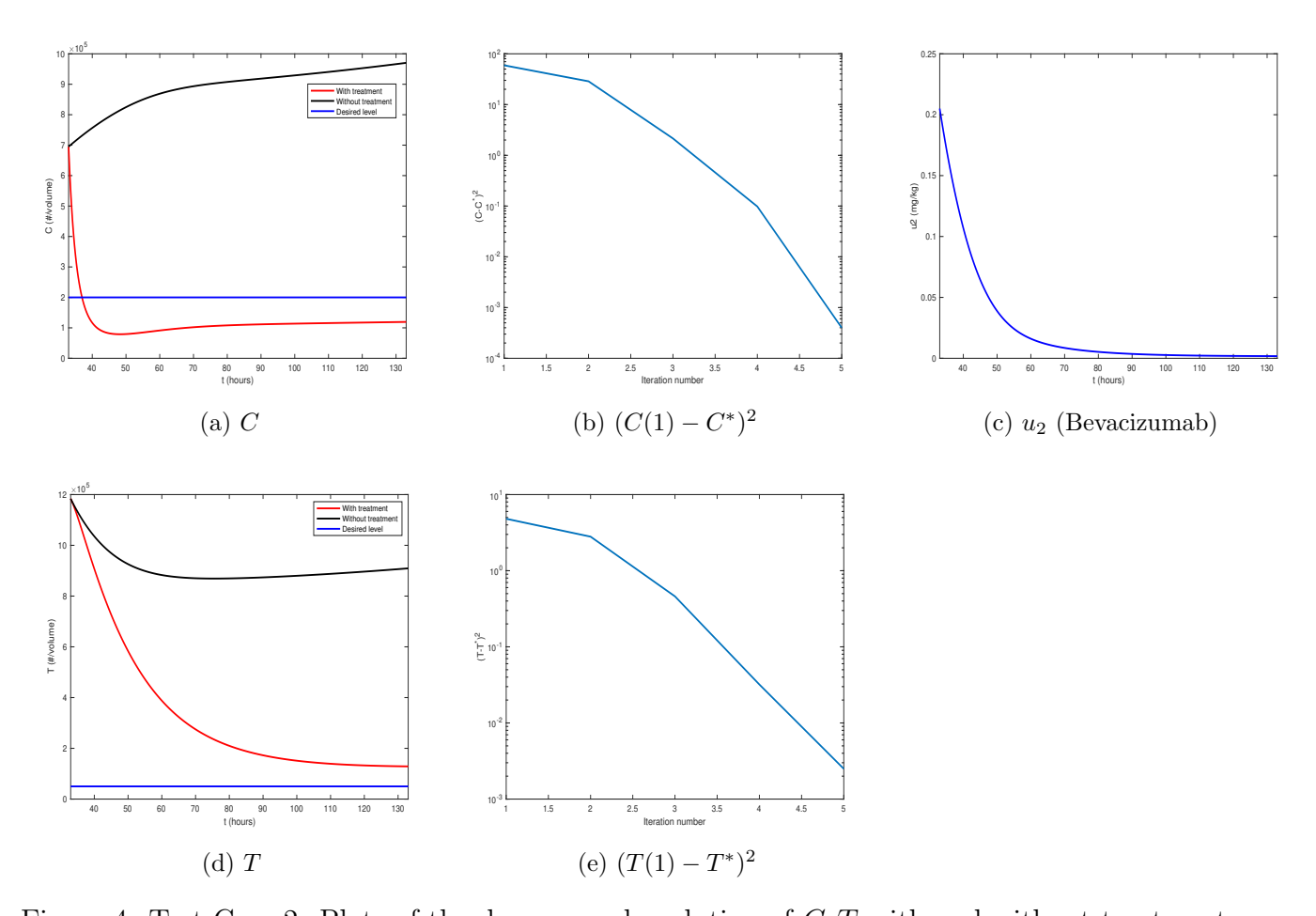


Figure 4: Test Case 2: Plots of the dosages and evolution of C, T with and without treatments.

We again observe that the without treatment, the values of C, T increase, whereas with the treatment u_2 , the values of C, T are driven towards the desired levels. Furthermore, we also note from Figure 4(b) and (e), the evolution of $(C(T_f) - C^*)^2$, $(T(T_f) - T^*)^2$ during the optimal control process against the iterate number. We again observe a monotonic decrease till convergence is achieved.

5.1 Discussion

Through the aforementioned two test cases, we obtained a dynamic optimal dosage regime for patients with two different stages of EC. This dynamic treatment regime was obtained through a combination of a new ODE dynamical model for RTK signaling pathways and a sensitivity analysis approach to determine the number of drugs to be used for an individual patient. A final optimal control problem gives us the actual treatment regime and the corresponding outcomes. Such a setup is in contrary to existing treatment regimes with Trastuzumab and Bevacizumab for other cancer types like breast cancers, where the drugs are administered based on a fixed

schedule and dosage. Moreover, the current dosage schedule of the two drugs for breast cancer are as follows: Trastuzumab is administered with a loading dosage of 8mg/kg in the first week followed by maintenance dosage of 6mg/kg every three weeks. The standard treatment regime is 52 weeks [13]. Bevacizumab, on the other hand, is administered at a dosage of 10mg/kg for every 2 weeks (without combination of chemotherapy), with recommended continuation of treatment for a long time [15]. The drugs are administered in 1 day for every weekly schedule. We observe from the plots of the dosages in Figures 2 and 4 that the maximum dosage administered in 1 day for Trastuzumab is 2mg/kg in a 1 day period and for Bevacizumab is 3.73-5 mg/kg in a 1 day period, which is significantly lower than the traditional dosage. Furthermore, we also note that the total time period of treatment to achieve the desired results is approximately 5.5 days (less than week) in comparison to the aforementioned long treatment schedules. This shows that our obtained optimal treatment regime provides a lower maximum dosage and a shorter treatment schedule for treating EC patients, which will lead to the decrease in toxic side-effects and secondary risk factors.

6 Conclusions

In this paper, we presented a new framework for obtaining personalized optimal treatment strategies in EC. For this purpose, we modeled the dynamics of RTK signaling pathways using a new pharmacokinetic model that takes into account a specific extrinsic heterogeneity. We then solved an optimization problem to obtain the parameters of this model from noisy patient data. The numerical discretization of the forward and the adjoint equations were done using a second-order, elementary stable, and positive NSFD scheme. We also solved the optimality system using a projected NCG scheme. Furthermore, we performed a sensitivity analysis of the optimal parameters with respect to the sum of the bound EGFR and HER2 using the LHS-PRCC method. Using this analysis, we modified our pharmacokinetic model to incorporate two types of drugs, Trastuzumab and Bevacizumab. We finally solved an optimal control problem to obtain the optimal dosages that drive the number of bound EGFR and HER2 to a desired level. Numerical experiments with synthetic data demonstrated that our proposed framework can be used to obtained optimal combination therapies in real-time with high accuracy.

Acknowledgments

This work was funded by the National Science Foundation-Division of Mathematical Sciences (NSF-DMS) grant number 2212938 and UTA Interdisciplinary Research Grant number 2021-772. We also thank the anonymous reviewers whose suggestions have helped improve the quality of the work.

Data availability

The datasets generated during and/or analysed during the current study are available from the corresponding author on reasonable request.

References

- [1] Mario Annunziato and Alfio Borzì. A fokker–planck control framework for multidimensional stochastic processes. *Journal of Computational and Applied Mathematics*, 237(1):487–507, 2013.
- [2] Yoshifumi Baba, Daichi Nomoto, Kazuo Okadome, Takatsugu Ishimoto, Masaaki Iwatsuki, Yuji Miyamoto, Naoya Yoshida, and Hideo Baba. Tumor immune microenvironment and immune checkpoint inhibitors in esophageal squamous cell carcinoma. *Cancer science*, 111(9):3132–3141, 2020.
- [3] Fortunato Bianconi, Elisa Baldelli, Vienna Ludovini, Lucio Crino, Antonella Flacco, and Paolo Valigi. Computational model of egfr and igf1r pathways in lung cancer: a systems biology approach for translational oncology. *Biotechnology Advances*, 30(1):142–153, 2012.
- [4] Yan Chang, Marah Funk, Souvik Roy, Elizabeth Stephenson, Sangyong Choi, Hristo V Kojouharov, Benito Chen, and Zui Pan. Developing a mathematical model of intracellular calcium dynamics for evaluating combined anticancer effects of afatinib and rp4010 in esophageal cancer. *International Journal of Molecular Sciences*, 23(3):1763, 2022.
- [5] Chun Chen, William T Baumann, Robert Clarke, and John J Tyson. Modeling the estrogen receptor to growth factor receptor signaling switch in human breast cancer cells. *FEBS letters*, 587(20):3327–3334, 2013.
- [6] Amina Eladdadi and David Isaacson. A mathematical model for the effects of her2 overexpression on cell proliferation in breast cancer. Bulletin of mathematical biology, 70:1707–1729, 2008.
- [7] Amina Eladdadi and David Isaacson. A mathematical model for the effects of her2 over-expression on cell cycle progression in breast cancer. *Bulletin of mathematical biology*, 73:2865–2887, 2011.
- [8] Jiahui Fan, Zhenqiu Liu, Xianhua Mao, Xin Tong, Tiejun Zhang, Chen Suo, and Xingdong Chen. Global trends in the incidence and mortality of esophageal cancer from 1990 to 2017. *Cancer medicine*, 9(18):6875–6887, 2020.
- [9] M. Flourakis, V. Lehen'kyi, B. Beck, M. Raphael, M. Vandenberghe, F. V. Abeele, M. Roudbaraki, G. Lepage, B. Mauroy, and C. Romanin et. al. Orail contributes to the establishment of an apoptosis-resistant phenotype in prostate cancer cells. *Cell Death & Disease*, 1(9):e75–e75, 2010.

- [10] Jeroen JMA Hendrikx, John BAG Haanen, Emile E Voest, Jan HM Schellens, Alwin DR Huitema, and Jos H Beijnen. Fixed dosing of monoclonal antibodies in oncology. *The oncologist*, 22(10):1212–1221, 2017.
- [11] Roy S Herbst, David H Johnson, Eric Mininberg, David P Carbone, Ted Henderson, Edward S Kim, George Blumenschein Jr, Jack J Lee, Diane D Liu, Mylene T Truong, et al. Phase i/ii trial evaluating the anti-vascular endothelial growth factor monoclonal antibody bevacizumab in combination with the her-1/epidermal growth factor receptor tyrosine kinase inhibitor erlotinib for patients with recurrent non–small-cell lung cancer. *Journal of Clinical Oncology*, 23(11):2544–2555, 2005.
- [12] A. Hoare, D. G. Regan, and D. P. Wilson. Sampling and sensitivity analyses tools (sasat) for computational modelling. *Theoretical Biology and Medical Modelling*, 5(1):1–18, 2008.
- [13] Po-Hung Hsieh, Alec J Kacew, Marie Dreyer, Anthony V Serritella, Randall W Knoebel, Garth W Strohbehn, and Mark J Ratain. Alternative trastuzumab dosing strategies in her2-positive early breast cancer are associated with patient out-of-pocket savings. NPJ Breast Cancer, 8(1):32, 2022.
- [14] Keiko Itano, Takeshi Ito, Shuji Kawasaki, Yoshinori Murakami, and Takashi Suzuki. Mathematical modeling and analysis of erbb3 and egfr dimerization process for the gefitinib resistance. *JSIAM Letters*, 10:33–36, 2018.
- [15] Filis Kazazi-Hyseni, Jos H Beijnen, and Jan HM Schellens. Bevacizumab. *The oncologist*, 15(8):819, 2010.
- [16] Eunjung Kim, Jae-Young Kim, Matthew A Smith, Eric B Haura, and Alexander RA Anderson. Cell signaling heterogeneity is modulated by both cell-intrinsic and-extrinsic mechanisms: An integrated approach to understanding targeted therapy. *PLoS biology*, 16(3):e2002930, 2018.
- [17] Daniel C. Kirouac. How Do We "Validate" a QSP Model? CPT: Pharmacometrics & Systems Pharmacology, 7(9):547–548, sep 2018.
- [18] K. Kondratska, A. Kondratskyi, M. Yassine, L. Lemonnier, G. Lepage, A. Morabito, R. Skryma, and N. Prevarskaya. Orai1 and stim1 mediate soce and contribute to apoptotic resistance of pancreatic adenocarcinoma. *Biochimica et Biophysica Acta (BBA)-Molecular Cell Research*, 1843(10):2263–2269, 2014.
- [19] Gregoire F Le Bras, Muhammad H Farooq, Gary W Falk, and Claudia D Andl. Esophageal cancer: the latest on chemoprevention and state of the art therapies. *Pharmacological research*, 113:236–244, 2016.
- [20] Jacques-Louis Lions. Quelques méthodes de résolution de problemes aux limites non linéaires. 1969.

- [21] Simeone Marino, Ian B Hogue, Christian J Ray, and Denise E Kirschner. A methodology for performing global uncertainty and sensitivity analysis in systems biology. *Journal of theoretical biology*, 254(1):178–196, 2008.
- [22] AM Namboodiri and JP Pandey. Differential inhibition of trastuzumab-and cetuximab-induced cytotoxicity of cancer cells by immunoglobulin g1 expressing different gm allotypes. Clinical & Experimental Immunology, 166(3):361–365, 2011.
- [23] Guilian Niu, Kenneth L Wright, Mei Huang, Lanxi Song, Eric Haura, James Turkson, Shumin Zhang, Tianhong Wang, Dominic Sinibaldi, Domenico Coppola, et al. Constitutive stat3 activity up-regulates vegf expression and tumor angiogenesis. *Oncogene*, 21(13):2000–2008, 2002.
- [24] Emmanuelle Norguet, Laetitia Dahan, and Jean-Francois Seitz. Targetting esophageal and gastric cancers with monoclonal antibodies. Current topics in medicinal chemistry, 12(15):1678–1682, 2012.
- [25] Suvra Pal and Souvik Roy. A new non-linear conjugate gradient algorithm for destructive cure rate model and a simulation study: illustration with negative binomial competing risks. Communications in Statistics: Simulation and Computation, 2020.
- [26] Suvra Pal and Souvik Roy. On the estimation of destructive cure rate model: A new study with exponentially weighted Poisson competing risks. *Statistica Neerlandica*, 2021.
- [27] Z. Pan and J. Ma. Open sesame: treasure in store-operated calcium entry pathway for cancer therapy. *Science China Life sciences*, 58(1):48–53, 2015.
- [28] Francesco Pappalardo, Giulia Russo, Saverio Candido, Marzio Pennisi, Salvatore Cavalieri, Santo Motta, James A. McCubrey, Ferdinando Nicoletti, and Massimo Libra. Computational modeling of pi3k/akt and mapk signaling pathways in melanoma cancer. PLOS ONE, 11(3):1– 10, 03 2016.
- [29] Efstathios T Pavlidis and Theodoros E Pavlidis. Role of bevacizumab in colorectal cancer growth and its adverse effects: a review. World journal of gastroenterology: WJG, 19(31):5051, 2013.
- [30] Christina Plattner and Hubert Hackl. Modeling therapy resistance via the egfr signaling pathway. *The FEBS journal*, 286(7):1284–1286, 2019.
- [31] Souvik Roy, Mario Annunziato, and Alfio Borzì. A fokker-planck feedback control-constrained approach for modelling crowd motion. *Journal of Computational and Theoretical Transport*, 45(6):442–458, 2016.
- [32] Souvik Roy, Mario Annunziato, Alfio Borzì, and Christian Klingenberg. A fokker–planck approach to control collective motion. *Computational Optimization and Applications*, 69(2):423–459, 2018.

- [33] Souvik Roy, Zui Pan, and Suvra Pal. A fokker–planck feedback control framework for optimal personalized therapies in colon cancer-induced angiogenesis. *Journal of Mathematical Biology*, 84(4):1–32, 2022.
- [34] Matthew W Short, Kristina Burgers, and Vincent Fry. Esophageal cancer. *American family physician*, 95(1):22–28, 2017.
- [35] Xiao-xiao Sun and Qiang Yu. Intra-tumor heterogeneity of cancer cells and its implications for cancer treatment. *Acta Pharmacologica Sinica*, 36(10):1219–1227, 2015.
- [36] Victoria E Wang, Jennifer R Grandis, and Andrew H Ko. New strategies in esophageal carcinoma: Translational insights from signaling pathways and immune checkpointsnew strategies in esophageal cancer. *Clinical Cancer Research*, 22(17):4283–4290, 2016.
- [37] N. Yang, Y. Tang, F. Wang, H. Zhang, D. Xu, Y. Shen, S. Sun, and G. Yang. Blockade of store-operated ca2+ entry inhibits hepatocarcinoma cell migration and invasion by regulating focal adhesion turnover. *Cancer Letters*, 330(2):163–169, 2013.
- [38] S. Yang, J. J. Zhang, and X-Y. Huang. Orail and stim1 are critical for breast tumor cell migration and metastasis. *Cancer Cell*, 15(2):124–134, 2009.
- [39] Connie Yip, David Landau, Robert Kozarski, Balaji Ganeshan, Robert Thomas, Andriana Michaelidou, and Vicky Goh. Primary esophageal cancer: heterogeneity as potential prognostic biomarker in patients treated with definitive chemotherapy and radiation therapy. *Radiology*, 270(1):141–148, 2014.
- [40] H. Zhu, H. Zhang, F. Jin, M. Fang, M. Huang, C. S. Yang, T. Chen, L. Fu, and Z. Pan. Elevated orai1 expression mediates tumor-promoting intracellular ca2+ oscillations in human esophageal squamous cell carcinoma. *Oncotarget*, 5(11):3455, 2014.
- [41] Huixi Zou, Parikshit Banerjee, Sharon Shui Yee Leung, and Xiaoyu Yan. Application of pharmacokinetic-pharmacodynamic modeling in drug delivery: development and challenges. *Frontiers in pharmacology*, 11:997, 2020.